PAPER

High temperature ferromagnetic resonance study on pMTJ stacks with diffusion barrier layers

IOP Publishing Journal of Physics D: Applied Physics
J. Phys. D: Appl. Phys. **51** (2018) 405001 (7pp) https://doi.org/10.1088/1361-6463/aad94e

High temperature ferromagnetic resonance study on pMTJ stacks with diffusion barrier layers

W C Law[1,2], T Tahmasebi[2], F N Tan[1,2], T L Jin[1], W L Gan[1], R R Nistala[2], X T Zhu[2], Z Q Mo[2], H W Teo[2], C S Seet[2], A See[2], S N Piramanayagam[1] and W S Lew[1,3]

[1] School of Physical and Mathematical Sciences, Nanyang Technological University, Singapore 637371, Singapore
[2] GLOBALFOUNDRIES Singapore Pte, Ltd., Singapore 738406, Singapore

E-mail: wensiang@ntu.edu.sg

Received 24 May 2018, revised 30 July 2018
Accepted for publication 9 August 2018
Published 29 August 2018

Abstract

We investigate the impact of Ru, Mo and W as an insertion layer between the second MgO and the top electrode in dual-MgO pMTJ stacks on the free layer magnetic properties from 25 °C to 260 °C. The insertion of Ru helps to improve the room temperature thermal stability by 97% in comparison to the control sample as its closely packed structure and large grain size suppresses interlayer diffusion. The effective anisotropy field (H_{eff}) of these samples were found to decay linearly at an increased rate as compared to the areal moment ($M_s t$) for the range of temperature measured through high temperature ferromagnetic resonance spectrometer and vibrating sample magnetometer. Furthermore, the extrapolated H_{eff} values across all samples having the same free layer composition converge towards zero at $T = 325$ °C, independent of the initial H_{eff} values measured at room temperature. Our measurement reveals that the free layer saturation magnetization plays a more significant role than H_{eff} in achieving higher thermal stability at typical MRAM operating temperatures.

Keywords: pMTJ, thermal stability, ferromagnetic resonance, magnetic anisotropy, diffusion barrier

(Some figures may appear in colour only in the online journal)

Introduction

Magnetoresistive random access memory (MRAM) has been the focus in both academia and industry as the emerging technology for embedded memory applications due to its speed, endurance, non-volatility, scalability and ease of integration with CMOS technology [1–4]. At the core of the MRAM lies the array of magnetic tunnel junctions with perpendicular magnetic anisotropy (pMTJ), which requires stringent deposition conditions and intricate stack design. In a pMTJ utilizing CoFeB as the free layer, the film interfaces and crystallinity are key factors in promoting high perpendicular magnetic anisotropy (PMA) and high tunnel magnetoresistance (TMR) ratio [3–12]. In addition, the pMTJ stack should have the thermal robustness to withstand the 400 °C annealing temperature in order to be compatible with CMOS-BEOL processes [13–16].

Various stack designs have since been reported to improve on different aspects of device functionality, such as dual-MgO pMTJ stack with an insertion layer between two CoFeB layers to maximise the TMR and thermal stability [9, 15–19]. Ta has been a conventional choice for such insertion layers and electrode contacts due to its low resistivity, amorphous nature and boride scavenging properties, allowing it to break crystalline texture for subsequent over layers. However, Ta has been reported to be highly diffusive after 400 °C annealing

[3] Author to whom any correspondence should be addressed.

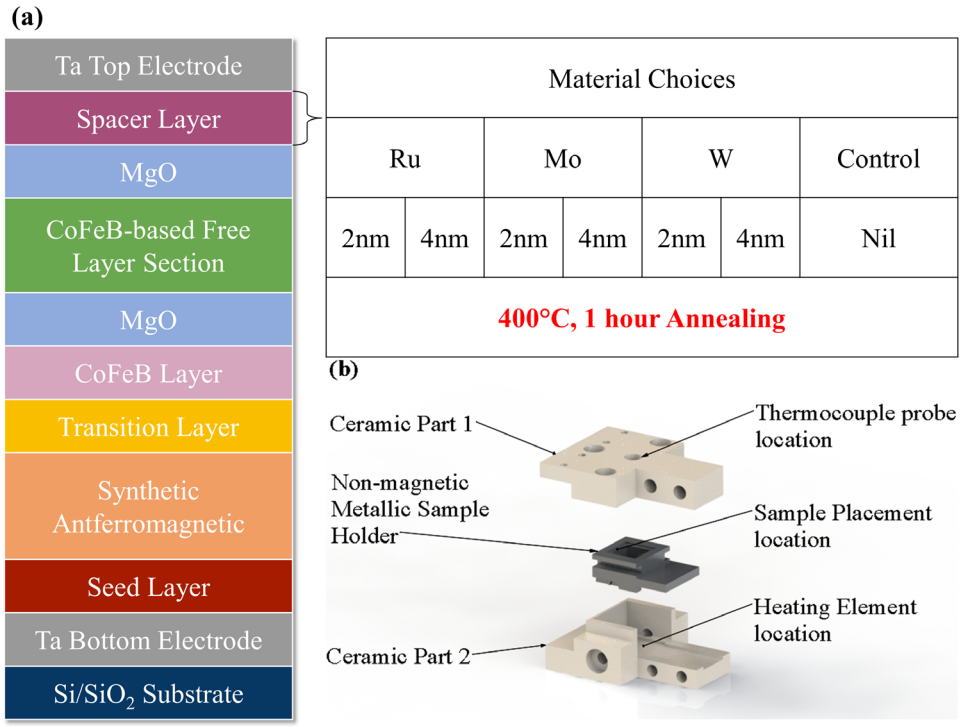

Figure 1. (a) Stack layout and (b) schematic of the test fixture in exploded view. There is no spacer layer present for the case of the control wafer, i.e. the second MgO is capped directly with the Ta top electrode.

treatment, which can result in interlayer mixing or the formation of the magnetically dead layer leading to a reduction in the thermal stability factor [5, 20]. In order to resolve this challenge, Mo and W have been reported to provide higher performance when deployed as buffer or capping layers to single MgO-based pMTJ stack structure [3, 5, 8, 21]. However, little attention is given to the interface between the second MgO and Ta-based top electrode in a dual-MgO pMTJ stack design [7, 15, 22].

Since MRAM applications often operate above ambient temperature, the temperature dependence of the free layer magnetic properties should also be evaluated as it will affect the thermal stability of the pMTJ stack [23–26]. The thermal stability is defined as the ability to retain storage information for a given period (typically 10 years) under a given operating environment. The thermal stability can be expressed as:

$$\Delta = \frac{K_{\mathrm{eff}} V}{k_{\mathrm{B}} T} = \frac{H_{\mathrm{eff}} M_{\mathrm{s}} t A}{2 k_{\mathrm{B}} T} \tag{1}$$

where k_{B} is the Boltzmann constant, T is temperature, V is the magnetic volume expressed as product of area A and thickness t, $K_{\mathrm{eff}} = H_{\mathrm{eff}} M_{\mathrm{s}}/2$ is the effective anisotropy energy and M_{s} is the saturation magnetization. H_{eff} is the effective anisotropy field defined as:

$$H_{\mathrm{eff}} = N_z M_{\mathrm{s}} + \frac{2K_u}{M_{\mathrm{s}}}, \tag{2}$$

where the first term corresponds to the demagnetization contribution of an infinitely extended thin film and the second term corresponds to the contribution from perpendicular anisotropy K_u. Even though the linear trend of H_{eff} as a function of temperature has been reported for CoFeB thin films at ultra-low temperatures [27], the temperature dependence of H_{eff} of CoFeB-based free layer at elevated temperatures has yet to be reported.

Here, we present a study on the impact of Ru, Mo and W inserted between the top electrode and the second MgO tunnel barrier on the electrical and magnetic performance of the pMTJ thin film stacks. By keeping the same free layer composition and deposited thickness across the samples in our study, we are able to determine how H_{eff} evolves at elevated temperatures due to the presence of the insertion layers.

Methodology

Using a magnetron sputtering system with a base pressure lower than 10^{-8} Torr, a series of bottom-pinned dual-MgO pMTJ similar to [7, 14, 15] were deposited on thermally oxidized Si substrates. The control wafer consists of a Ta bottom electrode, a 6 nm thick seed layer with fcc crystallinity, a synthetic antiferromagnetic (SAF) structure consisting of Co/Pt multilayers exchange-coupled via an ultrathin Ru layer, a CoFeB polarizing layer coupled to the SAF structure via an ultrathin amorphous transition layer, a CoFeB-based free layer section sandwiched by two MgO tunnel barriers and a Ta top electrode as shown in figure 1(a). Additional wafers were deposited with different spacer layers (Ru, Mo and W) of nominal thicknesses $t = 2$ nm and 4 nm inserted between the top electrode and the second MgO tunnel barrier. The samples were then subjected to 400 °C field annealing for an hour under a 1 Tesla magnetic field before subsequent analysis in current

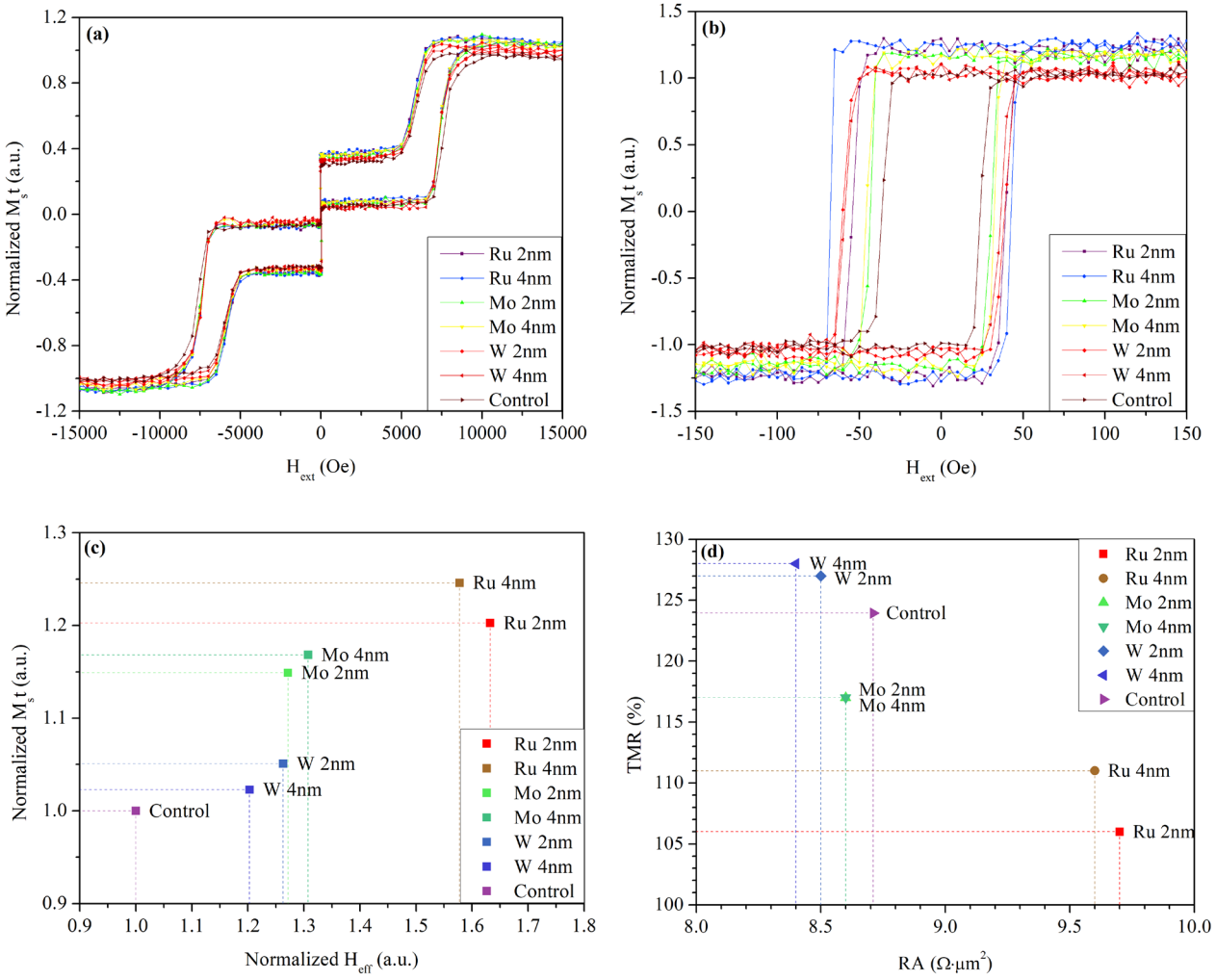

Figure 2. (a) Major loop and (b) minor loop VSM measurements. (c) $M_s t$ versus H_{eff} of the samples measured at room temperature. (d) Results of TMR and RA product from CIPT measurements.

in-plane tunnelling (CIPT) system, vibrating sample magnetometer (VSM) and vector network analyzer-ferromagnetic resonance spectrometer (VNA-FMR).

For the high temperature FMR measurement setup, the signal trace length for the grounded coplanar waveguide (GCPW) was elongated to minimize heat transfer to the end launch connectors [28, 29]. A ceramic jig was created to confine the heating to the sample, as well as a sample holder made of silver to minimize Oersted field arising from the ceramic heating element. A T-type surface thermocouple was placed on the back of the GCPW adjacent to the sample for PID temperature control. To verify that the thermocouple readings reflect the desired temperature, temperature labels from Testo were used to confirm that the temperature error was within the limits of the label itself (±1% +1 °C). Due to the limitation of the heating element and heat dissipation factor, a maximum of 260 °C was achieved for the HT-FMR setup, with the end launch connectors having a corresponding temperature of approximately 85 °C. Figure 1(b) shows the schematic view of the test fixture, which was then placed within an external magnetic field H_{ext} applied along the easy axis direction of the samples in the out-of-plane (OOP) configuration. All FMR measurements were fitted with the corresponding Kittel formula $f = \frac{\gamma}{2\pi}(H_{\text{ext}} + H_{\text{eff}})$ [9, 30, 31].

Results and discussion

Figures 2(a) and (b) shows the major and minor hysteresis loops respectively for the pMTJ stacks used in this study. The sharp switching of the free layers at the coercivity field is in good agreement with the high H_{eff} values obtained. The areal moment, $M_s t$, is obtained by dividing the magnetic moment from the minor hysteresis loops with the diced sample size having a square area of 16 mm^2. Figure 2(c) shows a summary overview of the magnetic properties of the free layer measured at room temperature, where the effective anisotropy field H_{eff} and the areal moment $M_s t$ were measured through VNA-FMR and VSM, respectively. All three material choices for insertion layers are able to significantly improve both $M_s t$ and H_{eff}. Specifically, the H_{eff} and $M_s t$ of the sample with Ru ($t = 4$ nm) insertion layer are ~159% and ~124%, respectively, as compared to the control wafer (normalized to as H''_{eff} and $M''_s t$). Since the $k_B T$ is the same for the room temperature results reported in figure 2(c), the insertion

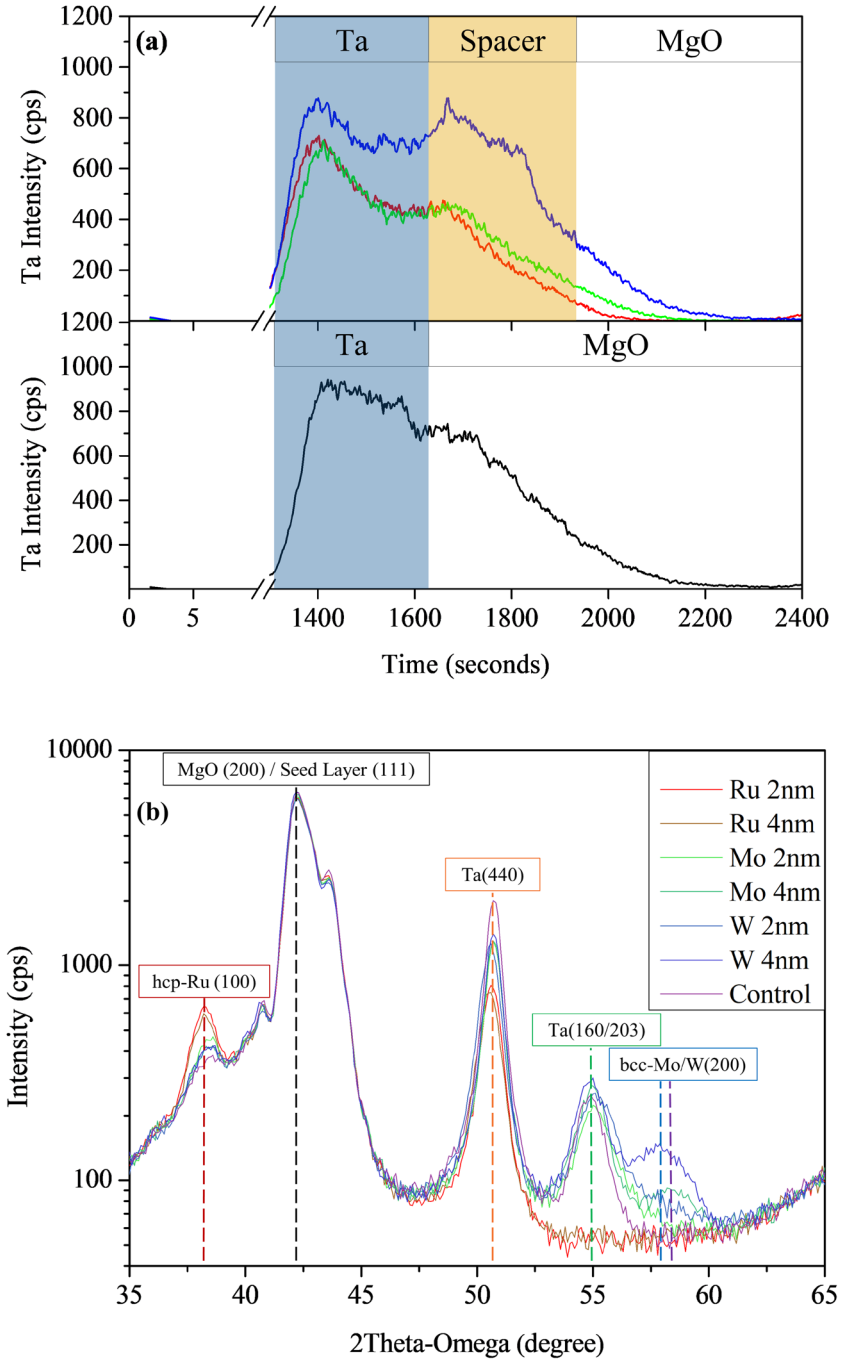

Figure 3. (a) TOF-SIMS analysis within the region of interest for selected samples. (b) XRD analysis for all samples showing enhanced peak at $2\theta = 38°$ for wafers with Ru insertions, while peaks were observed at $2\theta = 58°$ for wafers with W and Mo insertions.

of a 4 nm thick Ru spacer layer between the second MgO and Ta top electrode can increase the thermal stability by $\frac{\Delta_{Ru}-\Delta_{Control}}{\Delta_{Control}} \times 100\% = \frac{(1.59H''_{eff}*1.24M''_s t - H''_{eff}*M''_s t)}{H''_{eff}*M''_s t} \times 100\% = 97\%$, where Δ_{Ru} and $\Delta_{Control}$ refers to the thermal stability of the sample with Ru($t = 4$ nm) insertion layer and control wafer, respectively. This indicates that the insertion layers play a non-trivial role in retaining the structural integrity of the pMTJ stack at 400 °C. The material choice of the insertion layer rather than the thickness is the dominant factor, which could be due to the intrinsic crystalline and material properties. The variation in the free layer magnetic properties can be attributed to the extent of Ta diffusion through the different insertion layers, which would lead to the formation of magnetic dead layer effect and also have a detrimental effect on the crystallinity of the underlayers.

The samples were also tested for their magnetoresistive properties. Figure 2(d) shows the TMR and resistance-area product (RA) measured using CIPT. The control sample shows the desired properties such as largest TMR and the lowest RA. As a result of the insertion layers influencing the free layer magnetic properties, minor variations were observed in the TMR and RA. The variation in the electrical transport properties can be attributed to quality of the second MgO tunnel barrier affected by the diffusion of Ta top electrode, as well as the

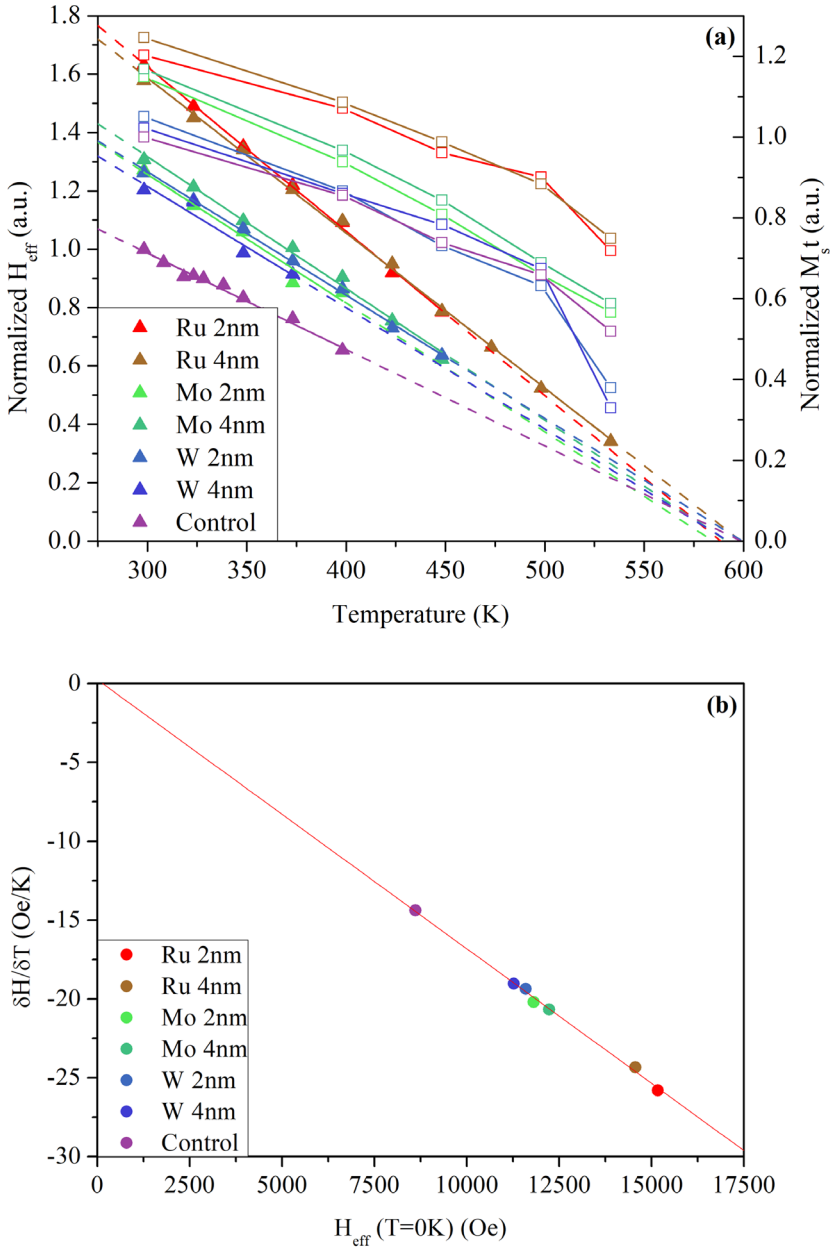

Figure 4. (a) $M_s t$ and H_{eff} as a function of temperature for each sample. Solid triangle symbols are H_{eff} obtained from HT-FMR measurements at elevated temperatures, while hollow square symbols are $M_s t$ obtained via HT-VSM. (b) Linear fit of $\frac{\partial H_{\text{eff}}}{\partial T}$ as a function of $H_{\text{eff}}(T = 0\,\text{K})$ based on the y-intercept and gradient of the straight line fitting results from (a).

extent of oxidation occurring at the interface between second MgO and the insertion layer.

As shown in figure 3(a), the depth profile from TOF-SIMS reveals the amount of Ta content within the MgO region. As the magnetic properties were not influenced by the thickness of the insertion layers, only wafers with 4 nm insertion layers as well as the control wafer are presented for clarity. We note that without an insertion layer present in the case of the control wafer, a significant amount of Ta diffuses into the MgO tunnel barrier. Qualitatively, increasing Ta content was observed within the MgO region in the order of Ru, Mo, W and finally the control wafer. This correlates with the hypothesis that suppression of Ta diffusion can lead to an improvement in the free layer magnetic performance.

The effect of different spacer layer material on the diffusion resistance can be explained by the grain size of the material choices [32]. Diffusion occurs through the grain boundaries and in the case of smaller grains, the ratio of grain boundary area to the volume is larger. A material with a larger grain size will have fewer grain boundaries and would show better diffusion resistance. Since the grain size is inversely proportional to the melting point, materials with a lower melting point would be more effective as diffusion barrier as these materials will have larger grains. Therefore, the larger grains formed by Ru are more likely to limit Ta from diffusing downwards as compared to materials with higher melting points such as Mo and W [33]. The results from XRD show that for the samples with Ru insertion layer, there is an increase in peak intensity at

$2\theta = 38°$ which corresponds to hcp-Ru in the 1 0 0 plane. This is in contrast to the broader peaks observed at $2\theta = 58°$ for samples with Ta and W capping layers. Base on the Scherrer equation [34], the peak widths obtained from the XRD results reveal that the grain size of Ru is larger than Ta and W and is more effective in limiting the diffusion of Ta.

The temperature dependence of magnetic properties for these samples were examined from room temperature up to 260 °C. As shown in figure 4(a), the rate of decay of $M_s t$ as a function of temperature, $\frac{\partial M_s t}{\partial T}$, of all the samples followed a hyperbolic relation in agreement with the mean field approximation. On the other hand, the rate of decay of effective anisotropy field as a function of temperature, $\frac{\partial H_{\text{eff}}}{\partial T}$, showed a linear decay in agreement with previous report on CoFeB thin films at ultralow temperature [27]. Moreover, $\frac{\partial H_{\text{eff}}}{\partial T}$ was found to be significantly larger than $\frac{\partial M_s t}{\partial T}$ within the measured range, with H_{eff} retaining a much lower percentage of their initial values at 260 °C as compared to $M_s t$. Lastly, the extrapolation of x-intercepts for all the samples from figure 4(a) leads to a convergence to a single temperature of $T_{H_{\text{eff}}} = 325$ °C despite different initial H_{eff} measured at room temperature, which can be attributed to the same free layer composition used in this study.

To explain the phenomenon behind a larger $\frac{\partial H_{\text{eff}}}{\partial T}$ seen with an improvement in H_{eff}, the definition of H_{eff} listed in equation (2) is extended to consider its temperature dependence:

$$H_{\text{eff}}(T) = N_z M_s(T) + \frac{2K_u(T)}{M_s(T)}, \tag{3}$$

where T within the parenthesis refers to temperature. Therefore, at absolute zero temperature, H_{eff} becomes:

$$H_{\text{eff}}(T = 0\,\text{K}) = N_z M_s(T = 0\,\text{K}) + \frac{2K_u(T = 0\,\text{K})}{M_s(T = 0\,\text{K})}. \tag{4}$$

Using the same approach as [27], the Cullen–Cullen power law is used to substitute the term $K_u(T)$ as a function of M_s and $K_u(T = 0\,\text{K})$ and the proportionality constant, Γ, is set to be 2 as described in previous works [35, 36]. The first order derivative of equation (3) with respect to temperature leads to:

$$\frac{\partial H_{\text{eff}}}{\partial T} = \frac{\partial M}{\partial T}\frac{1}{M_s(T = 0\,\text{K})}\left[N_z M_s(T = 0\,\text{K}) + \frac{2K_u(T = 0\,\text{K})}{M_s(T = 0\,\text{K})}\right]. \tag{5}$$

The terms within the square parenthesis are exactly similar to equation (4), which are replaced to obtain the following expression:

$$\frac{\partial H_{\text{eff}}}{\partial T} = \frac{\partial M}{\partial T}\left[\frac{1}{M_s(T = 0\,\text{K})}\right] H_{\text{eff}}(T = 0\,\text{K}), \tag{6}$$

where $\frac{\partial M}{\partial T}$ is the rate of change of M_s. Noting that equation (6) is based on the assumption that $\frac{\partial M}{\partial T}$ is constant in order for Γ to be 2, we should expect the fit of $\frac{\partial H_{\text{eff}}}{\partial T}$ against $H_{\text{eff}}(T = 0\,\text{K})$ to pass through the origin for samples with the same free layer composition (and therefore the same M_s at $T = 0\,\text{K}$). Indeed, by using the gradients and y-intercepts of the H_{eff} plot from figure 4(a) to compare $\frac{\partial H_{\text{eff}}}{\partial T}$ as a function of $H_{\text{eff}}(T = 0\,\text{K})$, the experimental results in figure 4(b) are in excellent agreement with equation (6) with the case of proportionality constant, $\Gamma = 2$ for CoFeB.

Conclusion

In conclusion, we have shown that the insertion of Ru spacer layer between the Ta-based top electrode and the MgO tunnel barrier can improve the thermal stability of the pMTJ stack by up to 97% at room temperature. This is due to the intrinsic material properties limiting Ta from diffusing downwards. The temperature dependence of H_{eff} of up to 260 °C is found to be linear and dependent on $H_{\text{eff}}(T = 0\,\text{K})$. $\frac{\partial H_{\text{eff}}}{\partial T}$ also decays much rapidly in comparison to $\frac{\partial M}{\partial T}$, resulting in a larger impact on the thermal stability of the pMTJ stack at elevated operating temperatures. Therefore, HT-FMR can be utilized as a material screening method to optimize free layer at blanket film level, providing feedback to pMTJ stacks undergoing 260 °C solder reflow temperature without a need for a long learning cycle arising from device patterning and integration with CMOS technology.

Acknowledgments

This work was supported by the Singapore National Research Foundation, Prime Minister's Office, under a Competitive Research Programme (Non-Volatile Magnetic Logic and Memory Integrated Circuit Devices, NRF-CRP9-2011-01), and an Industry-IHL Partnership Program (NRF2015-IIP001-001). The support from an RIE2020 AME-Programmatic Grant (No. A1687b0033) is also acknowledged. W S L is a member of the Singapore Spintronics Consortium (SG-SPIN).

ORCID iDs

W C Law https://orcid.org/0000-0002-1572-6694
F N Tan https://orcid.org/0000-0002-9646-2466
W L Gan https://orcid.org/0000-0001-9278-0718
S N Piramanayagam https://orcid.org/0000-0002-3178-2960
W S Lew https://orcid.org/0000-0002-5161-741X

References

[1] Chen E *et al* 2010 Advances and future prospects of spin-transfer torque random access memory *IEEE Trans. Magn.* **46** 1873–8
[2] Sbiaa R, Meng H and Piramanayagam S N 2011 Materials with perpendicular magnetic anisotropy for magnetic random access memory *Phys. Status Solidi* **5** 413–9
[3] Almasi H *et al* 2015 Enhanced tunneling magnetoresistance and perpendicular magnetic anisotropy in Mo/CoFeB/MgO magnetic tunnel junctions *Appl. Phys. Lett.* **106** 182406
[4] Diao Z *et al* 2007 Spin transfer switching in dual MgO magnetic tunnel junctions *Appl. Phys. Lett.* **90** 132508

[5] Liu T, Zhang Y, Cai J W and Pan H Y 2014 Thermally robust Mo/CoFeB/MgO trilayers with strong perpendicular magnetic anisotropy *Sci. Rep.* **4** 5895

[6] Barsukov I *et al* 2015 Magnetic phase transitions in Ta/CoFeB/MgO multilayers *Appl. Phys. Lett.* **106** 192407

[7] Lee D Y, Hong S H, Lee S E and Park J G 2016 Dependency of tunneling-magnetoresistance ratio on nanoscale spacer thickness and material for double MgO based perpendicular-magnetic-tunneling-junction *Sci. Rep.* **6** 38125

[8] Zhou J *et al* 2016 Large influence of capping layers on tunnel magnetoresistance in magnetic tunnel junctions *Appl. Phys. Lett.* **109** 242403

[9] Le Goff A, Soucaille R, Tahmasebi T, Swerts J, Furnemont A and Devolder T 2015 Optimization of top-pinned perpendicular anisotropy tunnel junctions through Ta insertion *Japan. J. Appl. Phys.* **54** 090302

[10] Frankowski M *et al* 2015 Buffer influence on magnetic dead layer, critical current, and thermal stability in magnetic tunnel junctions with perpendicular magnetic anisotropy *J. Appl. Phys.* **117** 223908

[11] Sinha J *et al* 2015 Influence of boron diffusion on the perpendicular magnetic anisotropy in Ta|CoFeB|MgO ultrathin films *J. Appl. Phys.* **117** 043913

[12] Engel C, Goolaup S, Teoh H K and Lew W S 2017 Effect of geometrical modulation on pMTJ magnetization reversal *IEEE. Trans. Magn.* **53** 7100707

[13] Lee S E, Takemura Y and Park J G 2016 Effect of double MgO tunneling barrier on thermal stability and TMR ratio for perpendicular MTJ spin-valve with tungsten layers *Appl. Phys. Lett.* **109** 182405

[14] Lee S E, Shim T H and Park J G 2016 Perpendicular magnetic tunnel junction (p-MTJ) spin-valves designed with a top $Co_2Fe_6B_2$ free layer and a nanoscale-thick tungsten bridging and capping layer *NPG Asia Mater.* **8** e324

[15] Couet S *et al* 2017 Impact of Ta and W-based spacers in double MgO STT-MRAM free layers on perpendicular anisotropy and damping *Appl. Phys. Lett.* **111** 152406

[16] Couet S *et al* 2016 Oxygen scavenging by Ta spacers in double-mgo free layers for perpendicular spin-transfer torque magnetic random-access memory *IEEE Magn. Lett.* **7** 3103004

[17] Sato H, Yamanouchi M, Ikeda S, Fukami S, Matsukura F and Ohno H 2012 Perpendicular-anisotropy CoFeB–MgO magnetic tunnel junctions with a MgO/CoFeB/Ta/CoFeB/MgO recording structure *Appl. Phys. Lett.* **101** 022414

[18] Sabino M P R, Sze T L and Tran M 2014 Influence of Ta insertions on the magnetic properties of MgO/CoFeB/MgO films probed by ferromagnetic resonance *Appl. Phys. Express* **7** 093002

[19] Devolder T *et al* 2016 Ferromagnetic resonance study of composite Co/Ni–FeCoB free layers with perpendicular anisotropy *Appl. Phys. Lett.* **109** 142408

[20] Soo Y J, Lim S H and Lee S R 2010 Magnetic dead layer in amorphous CoFeB layers with various top and bottom structures *J. Appl. Phys.* **107** 09C707

[21] Chatterjee J, Sousa R C, Perrissin N, Auffret S, Ducruet C and Dieny B 2017 Enhanced annealing stability and perpendicular magnetic anisotropy in perpendicular magnetic tunnel junctions using W layer *Appl. Phys. Lett.* **110** 202401

[22] Wang M *et al* 2018 Current-induced magnetization switching in atom-thick tungsten engineered perpendicular magnetic tunnel junctions with large tunnel magnetoresistance *Nat. Commun.* **9** 671

[23] Luc T, Jan G, Le S and Wang P 2015 Quantifying data retention of perpendicular spin-transfer-torque magnetic random access memory chips using an effective thermal stability factor method *Appl. Phys. Lett.* **106** 162402

[24] Slaughter J M *et al* 2016 Technology for reliable spin-torque MRAM products *2016 IEEE Int. Electron Devices Meeting (IEDM)* pp 21.5.1–4

[25] Song Y J *et al* 2016 Highly functional and reliable 8 Mb STT-MRAM embedded in 28 nm logic *2016 IEEE Int. Electron Devices Meeting (IEDM)* pp 27.2.1–4

[26] Shih M C *et al* 2016 Reliability study of perpendicular STT-MRAM as emerging embedded memory qualified for reflow soldering at 260 °C *2016 IEEE Symp. on VLSI Technology* pp 1–2

[27] Fu Y *et al* 2016 Temperature dependence of perpendicular magnetic anisotropy in CoFeB thin films *Appl. Phys. Lett.* **108** 142403

[28] Luo F *et al* 2017 Simultaneous determination of effective spin-orbit torque fields in magnetic structures with in-plane anisotropy *Phys. Rev.* B **95** 174415

[29] Jin T, Kumar D, Gan W, Ranjbar M, Luo F, Sbiaa R, Liu X, Lew W S and Piramanayagam S N 2018 Nanoscale compositional modification in Co/Pd multilayers for controllable domain wall pinning in racetrack memory *Rapid Res. Lett.* (https://doi.org/10.1002/pssr.201800197)

[30] Harward I, O'Keevan T, Hutchison A, Zagorodnii V and Celinski Z 2011 A broadband ferromagnetic resonance spectrometer to measure thin films up to 70 GHz *Rev. Sci. Instrum.* **82** 095115

[31] Enobio E C I, Sato H, Fukami S, Matsukura F and Ohno H 2015 CoFeB thickness dependence of damping constants for single and double CoFeB–MgO interface structures *IEEE Magn. Lett.* **6** 5700303

[32] Nicolet M A 1978 Diffusion barriers in thin films *Thin Solid Films* **52** 415–43

[33] Shi J Z *et al* 2005 Influence of dual-Ru intermediate layers on magnetic properties and recording performance of Co Cr Pt–SiO_2 perpendicular recording media *Appl. Phys. Lett.* **87** 222503

[34] Langford J I and Wilson A J C 1978 Scherrer after sixty years: a survey and some new results in the determination of crystallite size *J. Appl. Crystallogr.* **11** 102–13

[35] Thiele J U, Coffey K R, Toney M F, Hedstrom J A and Kellock A J 2002 Temperature dependent magnetic properties of highly chemically ordered $Fe_{55-x}Ni_xPt_{45}L_{10}$ films *J. Appl. Phys.* **91** 6595

[36] Mryasov O N, Nowak U, Guslienko K Y and Chantrell R W 2005 Temperature-dependent magnetic properties of FePt: effective spin Hamiltonian model *Europhys. Lett.* **69** 805–11